Journal of ELECTRONIC MATERIALS, Vol. 39, No. 9, 2010
DOI: 10.1007/s11664-010-1270-9

System Modeling and Validation of a Thermoelectric Fluidic Power Source: Proton Exchange Membrane Fuel Cell and Thermoelectric Generator (PEMFC-TEG)

MIN CHEN,[1,2] SØREN JUHL ANDREASEN,[1] LASSE ROSENDAHL,[1] SØREN KNUDSEN KÆR,[1] and THOMAS CONDRA[1]

1.—Institute of Energy Technology, Aalborg University, Pontoppidanstræde 101, 9220 Aalborg, Denmark. 2.—e-mail: mch@iet.aau.dk

To facilitate the co-design and co-optimization of fluid or combustion systems and thermoelectric devices, a three-dimensional (3D) thermoelectric generator (TEG) model has been proposed and implemented in a computational fluid dynamics (CFD) simulation environment. The model includes all temperature-dependent characteristics of the materials and nonlinear fluid–thermal–electric multiphysics coupled effects. In this paper, the device-level model is first extended to the module level by taking a general geometry, identifying regions such as positive and negative thermoelements, and assigning properties to them. The system-level model is then demonstrated by coupling the module-level model with a fluidic–thermal system model in a single CFD simulator to predict the generation performance based on the thermal equilibrium that is achieved. The linked models are validated experimentally at the system level using data from three real thermoelectric modules installed on the surface of an exhaust pipe-like rig, where the temperature profile as well as the electricity generated can be measured and compared with the simulation results. The rig is intended not only to verify the proposed system model but also to mimic a practical exhaust recovery apparatus for a proton exchange membrane fuel cell (PEMFC). Based on the data obtained from the system-level test rig, a novel low-temperature low-cost application for auxiliary electric power appliances based on the waste heat of the PEMFC can be envisaged. Within the common simulator, it is shown that the thermoelectric model can be connected to various continuum-domain CFD models of the fuel cell itself, thus enabling further possibilities to optimize system efficiency and performance.

Key words: CFD modeling, TEG, PEMFC, system-level testing, co-optimization

INTRODUCTION

In the investigation of TEG applications and system modeling, one important aspect is the assumption of a non-constant-temperature boundary condition on the device junctions. Based upon the macroscopic thermodynamic and one-dimensional (1D) analytical methodology, the effects of heat conduction and/or Joule generation across the interfaces between the thermoelectric device and the reservoirs have been extensively discussed.[1–4] In such 1D analytical models, the unrealistic assumption that the thermal resistances between heat reservoirs and TEG junctions are infinitesimal is removed. However, there are significant drawbacks related to another assumption, i.e., of constant-temperature boundary condition on the hot and cold

(Received June 26, 2009; accepted May 5, 2010; published online June 2, 2010)

reservoirs. Constant-temperature reservoirs simply mean infinite thermal mass, which is more or less idealized and not completely realistic for most TEG applications. In fact, any thermal or electric change in the TEG, as a special kind of thermal load applied on its hot and cold sides, will lead to a temperature response of abutting heat reservoirs if they are not infinite.

Attention has been paid to more general TEG models that include the reservoir scale.[5–7] Especially, by generalizing different hot and cold sources as fluids, different kinds of thermal energy systems with constant temperature can be numerically augmented so that more unknowns of the system status of both the TEG and the entire generating system can be resolved together in the popular CFD code FLUENT.[8] The 1D TEG model has been upgraded to a three-dimensional (3D) numerical model to reflect the influence of nonuniform heat flow and temperature distributions of fluid heat sources on TEG power and efficiency, as well as the coupled fluid–thermal–electric behavior of the system. Considering the application of a TEG in a combustion energy system, the impacts on thermoelectric generation of fluid properties such as flame temperature, fuel concentration, and supply rate can be included.

The original considerations, including full motivation, 3D model implementation, and device-level validation, have been documented in Ref. 8. This work demonstrates how to utilize the proposed TEG model to implement the CFD system model. Commercially available TEG modules with thermoelectric materials of known temperature-dependent properties have been incorporated into a laboratory test rig to furnish system-level measurements and a verification framework for the CFD model. We also consider the optimization of different thermal energy systems for TEG applications, and here a representative example, PEMFC exhaust utilization, has been modeled and analyzed.

CFD MODELING OF TEG SYSTEM

The 3D TEG model is implemented in the popular CFD package FLUENT 6.3, where the solid thermoelectric phenomena are solved by developing user-defined functions (UDF) in the ANSI C language.[8] User-defined scalars (UDS) are used to determine the electric field caused by the Seebeck potential and electric current throughout the thermoelements. The model includes the temperature dependence of all properties of the *p*- and *n*-type materials, and provides 3D profiles of temperature, Seebeck potential, and current density as well as the values of TEG power and efficiency. Comparisons with other modeling and device-level experimental results have validated the accuracy of the TEG model.[8] It is comprised of only a few UDF and UDS and is hence very scalable and flexible for incorporation into FLUENT, serving as an add-on module in parallel with other power source modules[9] provided within FLUENT. The TEG model is especially useful for co-design of the whole power system, because CFD submodels of fluid flow and combustion in FLUENT can be immediately connected to the TEG model as a continuum domain, thereby avoiding problems associated with multidimensional boundary condition translation in the fluid–structure coupling.

In order to apply the TEG model, there are a series of general steps to follow in FLUENT in addition to loading of the UDF and UDS:

- Create *p*- and *n*-type thermoelectric materials and define their temperature-dependent thermal conductivity and electric conductivity (UDS diffusivity);
- Create the metal material for conducting bridges and define its thermal and electric conductivities (UDS diffusivity);
- Modify the temperature-dependent Seebeck coefficients and initial values in UDF;
- Select applicable solid zones for each UDS;
- Apply boundary conditions, where source terms must be applied to appropriate solids, and the top and bottom interfaces between conducting bridges and *p*- and *n*-type legs must be set to include coupling between continuum thermal and electric (UDS) fields.

From the system modeling viewpoint, the implementation of 3D thermoelectric governing equations for a single couple must first be extended to the module level. Figure 1 shows the full 3D solid model and the grid of the 127 thermoelectric couple module (TEC1-12706) used in the device-level validation.[8] In such a module model, all *p*-type legs, all *n*-type legs, all top metal conducting bridges, and all bottom metal conducting bridges are specified as individual zone types, respectively. Thus the linking of various materials and UDF source terms to corresponding solids can be done easily in FLUENT without repeating them for each of the 127 couples. The exception to this is the exposed pads at the two corners, simulating the lead wires of the TEG. These cannot be specified in the same zone as other bottom metal conducting bridges, because electrical boundary conditions must be applied on them: one is connected to ground (specified value of UDS), and on the other, a calculated current (specified flux of UDS) is applied in each iteration. The current is calculated in terms of the overall built-in Seebeck potential, which is a sum of the potentials (UDS) across all *p*- and *n*-type legs. The 3D thermal and electric fields of the device in Fig. 1 can be obtained by following the aforementioned steps, but an important difference between modeling single- and multicouple TEG appears as the convergence speed of the UDS iteration slowing down. According to the general theory described by the FLUENT documentation, there are a number of options in regard to convergence acceleration, but simple numerical

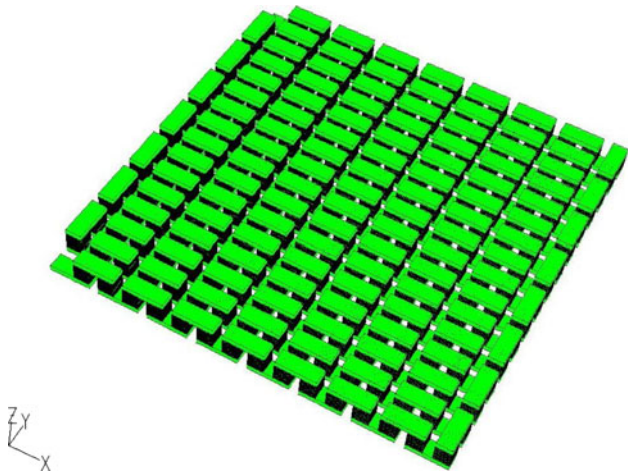

Fig. 1. Solid model and grid of a TEC1-12706 thermoelectric module.

experiments showed that, in this case, using a double-precision solver (3DDP) instead of a single-precision solver can normally increase the convergence speed to an acceptable level.

However, the system modeling described herein must include the interaction of the TEG model of three such modules with a demonstrative CFD submodel of a hexagonal fluid tube that emulates the exhaust pipe of the PEMFC as the hot source. The difficulty in convergence becomes more obvious when the many thermocouples of the three modules are connected in series and simulated by a single UDS, even when the double-precision solver is adopted. The transfer of the electric potential (UDS) boundary condition through such a long set of thermocouples seems to be the cause of the convergence problems. Therefore, two additional UDSs were created so that the electric potential distribution following Ohm's law within each module is simulated by an individual UDS. Not only has this solution proven feasible in terms of the convergence problem, but it is also reasonable in practice, because it is unlikely in any real application that all thermocouples would be connected in series, due to the undesirable possibility of device failure. Mostly, TEG thermocouples are grouped into modules, and it is certainly a fair strategy to apply one UDS for each electric potential distribution without increasing the model size. Of course the electrical configuration of the modules remains flexible (in series, in parallel, or hybrid) and can be specified by coding the boundary condition overlap in the UDF.

To mitigate the required computational effort, meshing optimization needs to be considered at the device level to reduce the total number of nodes.[8] In system models, however, there are a couple of additional meshing issues. The first arises due to the typical TEG design, which consists of many thermocouples. Thus, the interfaces between the TEG and the system must be split by a lot of holes to enable coupled heat transfer. Directly splitting this kind of face shape may be problematic in CFD preprocessors such as Gambit, where indirect splitting can be used, i.e., splitting a large face into small faces and then each small face by the holes corresponding to p- and n-type legs. The second issue is the mesh for the system (fluid region), which generally must have larger cell size than that of the thermoelectric region for an operational total model size. Such meshes with different sizes can be applied on unconnected entities of equivalent topology to the thermoelectric region, and interface zones can be connected afterwards in FLUENT by defining the grid interface.

SYSTEM-LEVEL TEST RIG

System-level test rigs are usually built on cold fluid tubes to cool the cold side of the TEG modules.[10,11] To validate the proposed numerical modeling, in this work a simple system-level test rig mainly emulating the hot air flow conditions of a fuel cell stack was constructed. The designed setup can also be used to estimate the potential power output and efficiency of a series of TEG modules or pellets spatially distributed for other similar applications. The system setup is shown in Fig. 2.

In order to emulate the exhaust air flow of a fuel cell stack, a Bürkert 8626 mass flow controller was used to specify an air flow varying from 0–300 L/min. The temperature of the air exiting the mass flow controller can be controlled by a Leister LHS20L/System three-phase air heater. It is able to deliver up to 3 kW of power to the incoming air, and the temperature can be controlled at the desired emulation temperatures, mostly in the range of 300 K to 475 K but maybe higher. The hot air enters the hexagonal aluminum exhaust pipe, where three TEC1-12706 modules are mounted on its top surface, with 12 type T thermocouples distributed evenly under the three modules. Furthermore, at the pipe inlet and outlet, aluminum wall and pipe center temperatures are measured.

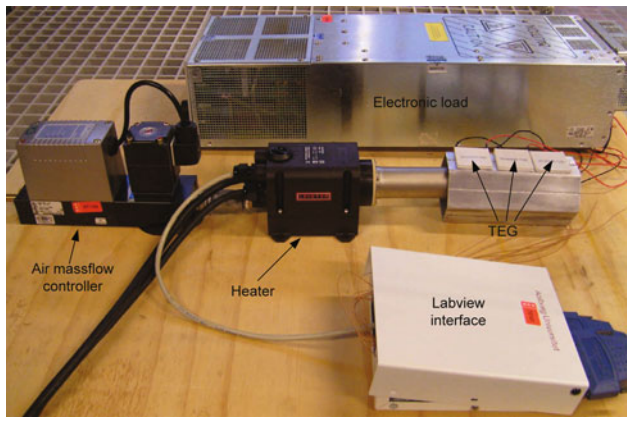

Fig. 2. Experimental setup for model validation.

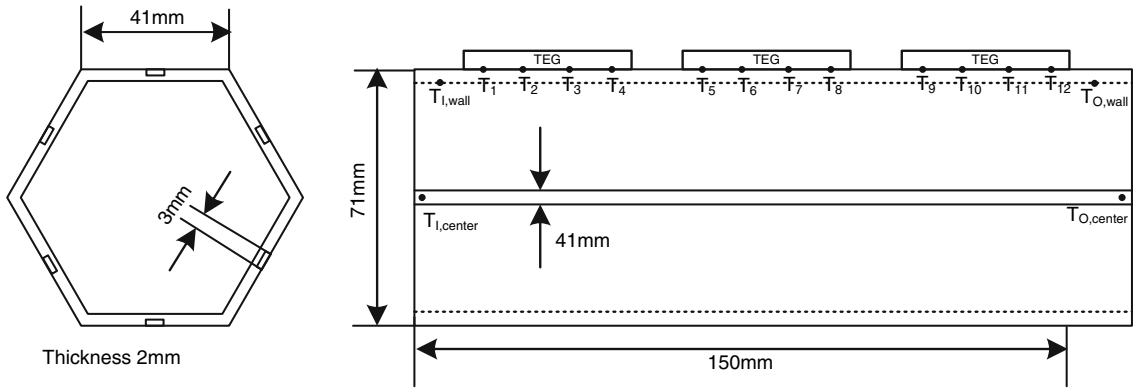

Fig. 3. Sketch of aluminum pipe for TEG mounting used to verify numerical model.

Figure 3 shows the dimensions of the aluminum pipe and the positions of the thermocouples.

The hexagonal shape of the aluminum pipe is dimensioned to be used as an exhaust pipe extension on a Serenergy 1-kW PEM fuel cell stack which will be presented later on. In each of the six sides of the hexagon, a 1-mm-deep channel is made in the 2-mm-thick aluminum wall to accommodate the thermocouples indicated in Fig. 3. The thermocouples are mounted using thermal conductive paste to maximize conduction. The pipe inlet temperature $T_{\mathrm{I,center}}$, is used to control the inlet temperature of the air entering the pipe, independently of the airflow. In this way, the setup can be used to verify the developed numerical model as well as the performance of TEG power generation.

PRELIMINARY RESULTS

Figure 4 shows the results of the module-level simulation for the electric potential variation caused by current flowing through the TEG module, i.e., the continuum electric potential distribution caused by the internal resistance of the TEG module (Ohm's law), where constant-temperature boundaries are applied on the top and bottom surfaces. The TEG module used (TEC1-12706) has a cross-section of 40 mm × 40 mm, and the *n*- and *p*-legs inside have dimensions of length × width × height = 1.4 mm × 1.4 mm × 1.6 mm. These dimensions as well as the thermal and electrical contact resistances are included in the model, where uniform boundary temperatures of 423 K and 303 K are assumed on the top and bottom surfaces, respectively, for the result in Fig. 4. In experimental measurements, a thin-film electrical heater is used to provide the specified temperature difference. With a roughly matched load, the extent of agreement between the measurements and the simulation results in terms of the main performance parameters such as output power and efficiency can be found and discussed, similarly to previous work.[8] To highlight the unique feature of this module-level model, i.e., that the internal resistance of the TEG module can be

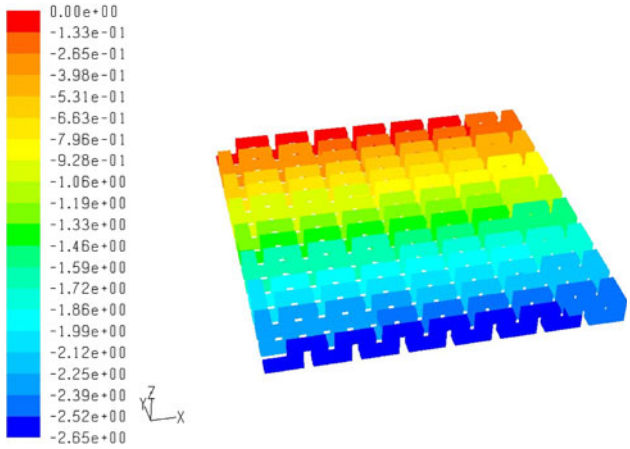

Fig. 4. Three-dimensional electric potential distribution resulting from the current generated in the TEG module for a temperature difference of 120 K.

calculated without scaling, a list of resistance values under various temperatures is presented in Table I. Note that the measured TEG resistance is based on the open-circuit voltage and short-circuit current at the same temperature setting, and the calculated values are obtained in terms of the multidimensional and temperature-dependent electrical resistivities of the *n*- and *p*-type materials. When temperatures of 423 K and 303 K are assumed on the two sides of the TEG module, the product of the internal resistance and the current is 2.6535 V. This Ohmic relation is shown multidimensionally in Fig. 4, where the red side mimics the ground and the blue side displays the voltage drop due to the generated current.

The system-level simulation was demonstrated by running a CFD submodel of the emulated exhaust and the hexagonal tube together with the TEG model of the three TEC1-12706 modules using FLUENT (Fig. 5). For simplicity, although the actual situation is not exactly the same, only the laminar solver and fully developed flow are considered preliminarily. For the air flow inlet, 500 K and

Table I. Comparison of measurements and module-level simulation results of the internal resistance of the TEG module; T_c = 303 K, R_{load} = 3.4 Ω

T_h [K]	Resistance (Simulation) [Ω]	Resistance (Measurement) [Ω]	Current (Simulation) [A]	Current (Measurement) [A]
423	2.9	3	0.915	0.856
403	2.77	2.82	0.78	0.745
383	2.64	2.75	0.637	0.618
363	2.51	2.66	0.485	0.48
343	2.4	2.52	0.327	0.333

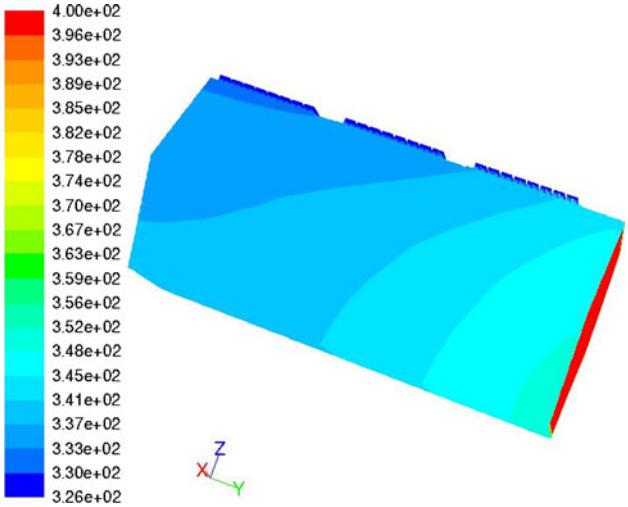

Fig. 5. Temperature distribution of a combined CFD model of the TEG and the exhaust tube.

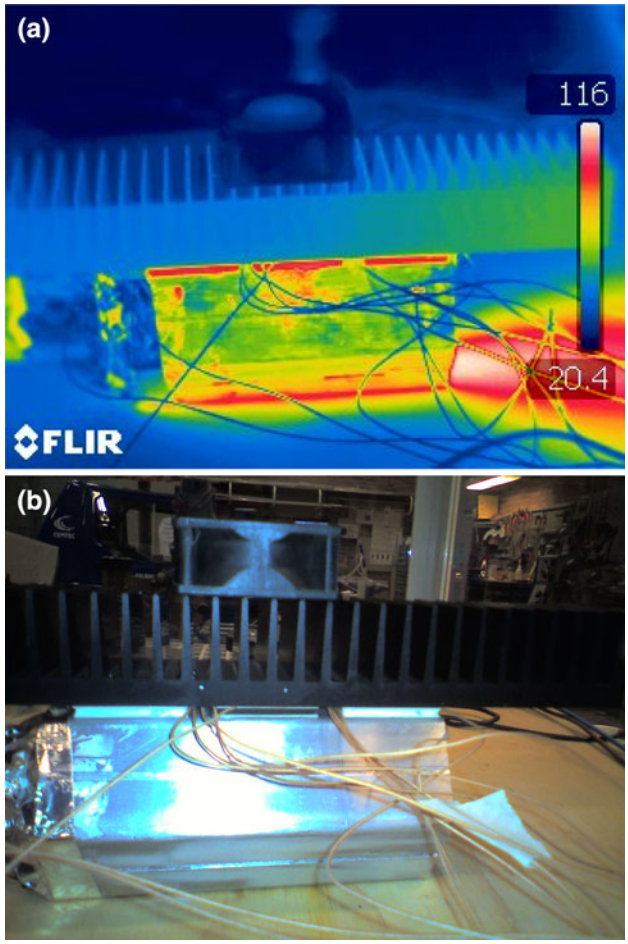

Fig. 6. The running experimental setup: (a) temperature distribution, and (b) close-up photograph.

1 m/s are assumed as the boundary conditions, measured by a thermocouple hung in the inlet air and the flow sensor in the mass controller, respectively. For the thermal boundary condition of the TEG model, in this application, the hot side must be coupled to the pipe as well as to the flowing air. The traditional methodology to treat such a coupled model is to model the fluids independently using CFD technique, followed by use of the CFD thermal analysis results to calculate the TEG power output. Now that the TEG modeling has been implemented in the CFD simulator, the combined effects on generation performance of the input energy flow to the hot source (air supply rate and temperature, for example), the output energy flow from the cold source, and the dynamic heat exchange ability of the sources can be automatically included in the single solver (FLUENT).

In the experimental setup, natural convection is initially assumed as the cold source. As expected, the three different modules perform differently due to the nonuniform hot-side surface temperature. For example, the open-circuit voltage of the middle TEG module is measured as 0.47 V, whereas that of the module next to the outlet is only 0.37 V. The system temperature profile of the pipe shell shown in both the simulation data (Fig. 5) and the experimental results (Fig. 6) can be used to explain this difference. In order to increase the temperature difference across the TEG for more power, an aluminum heat sink was attached to the cold side of the TEG to enhance convection, where fans can be further mounted to replace natural convection with forced convection. Regarding the model boundary at the cold side, however, the actually measured temperature is used, since it is difficult to estimate the exact heat transfer coefficient in the laboratory.

Table II. Comparison of measurements and system-level simulation results of the power performance of the middle TEG module

Cooling Method	$R_{load\ [\Omega]}$	Measured Current [A]	Simulated Current (T_{inlet} = 500 K) [A]	Simulated Current (T_{inlet} = 450 K) [A]	Simulated Current (T_{inlet} = 400 K) [A]
Natural convection ($T_c \approx 358$ K)	1.25	0.038	0.145	0.061	0.026
Natural convection (with heat sink, $T_c \approx 326$ K)	1.25	0.09	0.278	0.18	0.092
Forced convection ($T_c \approx 317$ K)	1.25	0.095	0.316	0.222	0.128

Although it is fairly feasible in both the model and the experiment to combine all three (or even more) modules our focus at this stage is on the middle module in order to study the power performance. The measurement and simulation results are shown in Table II. Under natural convection by air, when 500 K is assumed in the CFD model as the inlet temperature, it is found that the simulation results essentially overpredict. In fact, the temperature variation in the inlet of the hexagonal tube is very large, and at the edge positions of the inlet the temperature can be as low as 350 K. The temperature of 500 K mostly represents only the measurement at the center. Therefore, lower temperatures are applied to the inlet boundary condition to simulate the effects of the average temperature. It is shown in Table II that, when 400 K is adopted as the inlet temperature, measurement and simulation results are in good agreement. Further opportunities for modeling work thus becomes obvious, to extend the inlet and to explore turbulent CFD models to take into account more practical aspects, but the same concept of co-simulation with the TEG model can still be applied. The potential benefits of forced convection were also studied by running a fan on the heat sink and blowing air onto the middle module. It is interesting to find that, although the TEG cold-side temperature decreased by ~10 K, in this case the measured performance did not improve considerably (Table II). This may be because the TEG hot-side temperature also decreased. Figure 6a shows an infrared image of the experimental temperature profile of the pipe shell, based on which further optimization possibilities of various combinations of hot- and cold-side temperature distributions will be investigated in the future.

LOW-TEMPERATURE LOW-COST APPLICATION: PEMFC-TEG

Fuel cell systems are slowly entering the commercial market and appearing in more and more industrial products, such as back-up power supplies, auxiliary power units, and traction power for small electrical utility vehicles. Comparatively high-temperature PEM fuel cells work at operating temperatures of 430 K to 450 K, making cooling easier because the fuel cell polymer membrane is made from polybenzimidazole (PBI) instead of Nafion. The advantage is that liquid water is no longer needed to conduct protons through the membrane, but instead phosphoric acid allows the use of cathode air cooling.[12,13,14] Though these temperatures correspond to the low-temperature range of TEG applications, the overall system efficiency of fuel cell systems can still be improved by using the waste heat to produce electricity. These relatively higher temperatures[15] increase the feasibility of using a low-cost TEG (unit price < US $5) to generate electric power from the high-quality waste heat. Figure 7 shows the primary system components: an insulated 65-cell Serenergy 1-kW PEM fuel cell stack, the TEG exhaust pipe, the electronic load, and a Labview interface.

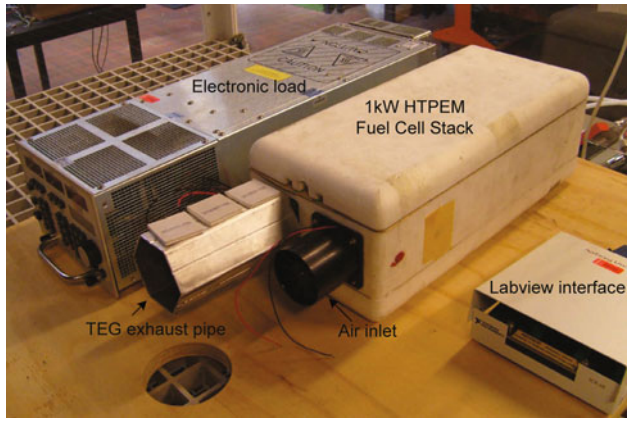

Fig. 7. PEMFC stack test setup with mounted TEG exhaust pipe.

Figure 8 shows the layout of the fuel cell system. The Labview interface is connected to a NI-8959 PCIe real-time data-acquisition system able to log the temperatures measured at different positions and to control the different system inputs and outputs. The PEMFC system is fuelled by pure hydrogen in a dead-end anode configuration at constant pressure of 0.2 bar through a pressure-reduction valve. During operation, the system is purged for 1 s at different adjustable intervals. The cathode is supplied with atmospheric air by a 24-V direct-current (DC) low-power axial blower. The cathode also acts as a cooling system, by increasing the air flow if the stack temperature increases above a

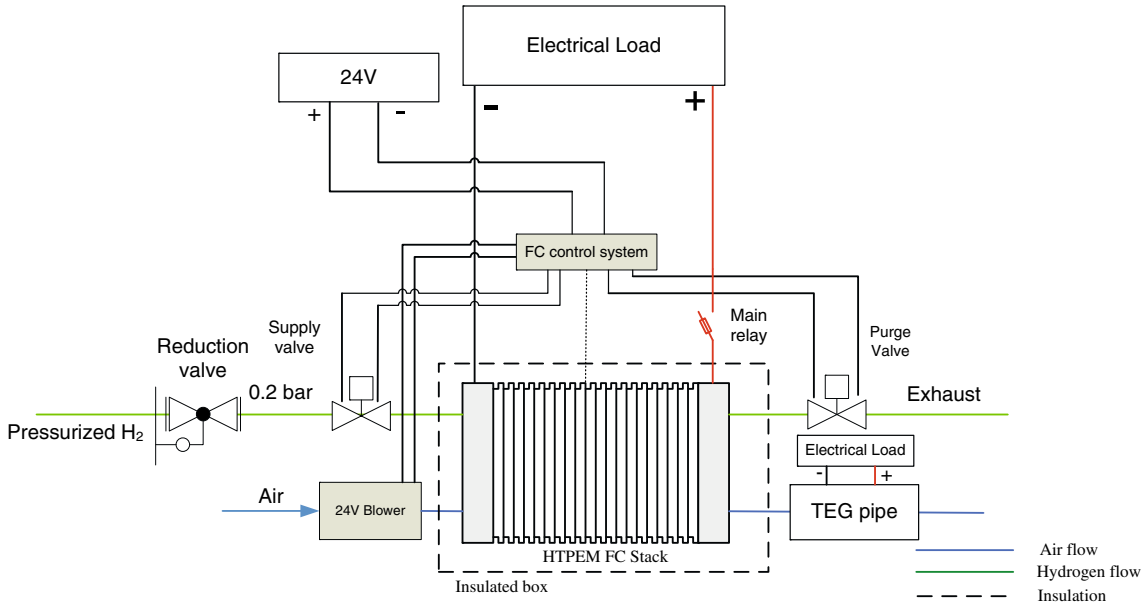

Fig. 8. PEMFC system hydrogen and airflow diagram.

specified setpoint temperature. In this way the stack temperature is controlled using the measured surface temperature of the middle fuel cell bipolar plate as controller feedback.

Because of the high temperature, it could be possible to supply auxiliary electrical power P_{aux} for the blower, valves, and control system by using the TEG on the exhaust pipe. This would increase the system power efficiency $\eta_{\text{FC,system}}$, which can be calculated as the ratio between the usable power and the actual power input:

$$\eta_{\text{FC,system}} = \frac{U_{\text{FC}} \cdot I_{\text{FC}} - P_{\text{aux}}}{\dot{m}_{\text{H}_2} \cdot LHV_{\text{H}_2}}, \quad (1)$$

where U_{FC} and I_{FC} are the fuel cell stack voltage and current, respectively. The input power can be calculated from the hydrogen mass flow $\dot{m}_{\text{H}_2}$ and LHV_{H_2}, which is the lower heating value of hydrogen. Removing the contribution of P_{aux} to the system efficiency by using the power from the TEG will certainly increase the fuel cell system efficiency.

CONCLUSIONS

In this paper, it is firstly shown that a CFD heat source model can be studied together with nonlinear thermoelectric effects in a single simulator. Therefore, research on the implementation of thermoelectricity in the CFD platform FLUENT by using UDF and UDS, as described in Ref. 8, has been clearly implemented successfully. Although some bug-fixing or other moderate changes in terms of special modeling contexts may be needed, future work on this approach lies solely in the system model, as all the essential problems at the device and module level have been solved.

A framework of co-simulation and co-optimization for a thermoelectric generation system has been proposed based on the proposed modeling. The CFD model of the exhaust pipe-like rig has been demonstrated to be able to run and couple with the TEG model in FLUENT as a whole. Preliminary system-level experiments have been attempted in order to furnish a verification tool for the simulation. More combined experiments of PEMFC-TEG (rather than separate experiments for PEMFC and TEG, respectively[15]) are to be carried out using the setup to confirm that the overall efficiency of the PEMFC can be improved. Detailed optimization of the heat-sink design, TEG location, exhaust tube shape/dimension, inlet and outlet temperature/mass rate, as well as their effects on the entire stack will be carried out following the proposed system modeling strategy. To include these aspects, the CFD sub-model needs to be further refined and extended. However, based on the TEG model already implemented in FLUENT and existing knowledge regarding the CFD platform, no problems for the development of such system models are envisaged.

ACKNOWLEDGEMENTS

This work is funded in part by the Danish Council for Strategic Research, Programme Commission on Energy and Environment, under Grant No. 2104-07-0053, and is carried out in the Center for Energy Materials in collaboration with Aarhus University, Denmark. The first author is also supported by the Danish Council for Independent Research and the Danish Council for Technology and Production Sciences, under Grant No. 09-069739. The authors are grateful to Jan Christiansen, Kim Nørgaard, and Danny Rabih Friwat for assistance

with the preparation of the experimental setup, and to Matthias Mandø for contributions to CFD modeling.

REFERENCES

1. M. Chen, S. Lu, and B. Liao, *J. Energy Resour. Trans. ASME* 127, 37 (2005).
2. P.M. Mayer and R.J. Ram, *Nanoscale Microscale Thermophys.* Eng. 10, 143 (2006).
3. T.J. Hendricks, *J. Energy Resour. Trans. ASME* 129, 223 (2007).
4. M. Freunek, M. Müller, T. Ungan, W. Walker, and L.M. Reindl, *J. Electron. Mater.* 38, 1214 (2009).
5. H.P.J. de Bock and V. Novak, *Proceedings of 11th Intersociety Conference on Thermal and Thermomechanical Phenomena in Electronic Systems (ITHERM)* (2008), pp. 1276–1282.
6. D.T. Crane and L.E. Bell, *J. Energy Resour. Trans. ASME* 131, 012401 (2009).
7. S.A. LeBlanc, Y. Gao, and K.E. Goodson, *Proceedings of ASME International Mechanical Engineering Congress and Exposition*, Vol. 8. (2009), pp. 131–137.
8. M. Chen (Ph.D. Dissertation, Aalborg University, 2009).
9. J.S. Herring, J.E. O'Brien, C.M. Stoots, G.L. Hawkes, J.J. Hartvigsen, and M. Shahnam, *Int. J. Hydrogen Energy* 32, 440 (2007).
10. E.F. Thacher, B.T. Helenbrook, M.A. Karri, and C.J. Richter, *Proc. IMechE. D: J. Automob. Eng*. 221, 95 (2007).
11. X. Niu, J. Yu, and S. Wang, *J. Power Sour.* 188, 621 (2009).
12. S.J. Andreasen and S.K. Kaer, *Int. J. Hydrogen Energy* 33, 4655 (2008).
13. S.J. Andreasen and S.K. Kaer, *J. Fuel Cell Sci. Tech. Trans. ASME* 6, 041006 (2009).
14. S.J. Andreasen, L. Ashworth, I.N.M. Remon, P.L. Rasmussen, and M.P. Nielsen, *Electrochem. Soc. Trans.* 12, 639 (2008).
15. D. Geng and C. Xie, *J. Power Sour.* (2010).